Statistical Analysis of the Preparatory Phase of the Mw 8.1 Iquique Earthquake, Chile

Florent Aden-Antóniow, Claudio Satriano, Pascal Bernard, Natalia Poiata, El-Madani Aissaoui, Jean-Pierre Vilotte, William B. Frank

JGR Solid Earth

RESEARCH ARTICLE
10.1029/2019JB019337

Statistical Analysis of the Preparatory Phase of the M_w 8.1 Iquique Earthquake, Chile

F. Aden-Antóniow[1,2], C. Satriano[2], P. Bernard[2], N. Poiata[2,3], E.-M. Aissaoui[2], J.-P. Vilotte[2], and W. B. Frank[1,4]

[1]Department of Earth Sciences, University of Southern California, Los Angeles, CA, USA, [2]Université de Paris, Institut de Physique du Globe de Paris, CNRS, Paris, France, [3]National Institute for Earth Physics, Magŭrele, Romania, [4]Department of Earth, Atmospheric and Planetary Sciences, Massachusetts Institute of Technology, Cambridge, MA, USA

Key Points:
- Evidences of a year-long preparatory phase of the Iquique earthquakes are found in a new seismic catalog
- A Kolmogorov-Smirnov one-sample test applied to the background seismicity suggests a large-scale acceleration of the seismicity rate
- A local Kolmogorov-Smirnov one-sample test reveals a seismic quiescence close to the Iquique earthquake coseismic rupture area

Supporting Information:
- Supporting Information S1

Correspondence to:
F. Aden-Antóniow,
adenanto@usc.edu

Citation:
Aden-Antóniow, F., Satriano, C., Bernard, P., Poiata, N., Aissaoui, E.-M., Vilotte, J.-P., & Frank, W. B. (2020). Statistical analysis of the preparatory phase of the M_w 8.1 Iquique earthquake, Chile. *Journal of Geophysical Research: Solid Earth*, *125*, e2019JB019337. https://doi.org/10.1029/2019JB019337

Received 3 JAN 2020
Accepted 6 MAY 2020
Accepted article online 12 MAY 2020

Abstract The 2014 Iquique seismic crisis in Chile, culminating with a M_w 8.1 earthquake on 1 April, highlights a complex unlocking of the Northern Chilean subduction that has been considered a seismic gap since 1877. During the year preceding this event, at least three clusters of seismic activity have been reported: in July 2013 and January and March 2014. Recent studies have proposed large-scale slab deformation as a potential trigger for the megathrust earthquake, and these clusters possibly indicate aseismic slip transients accompanying the progressive destabilization of the plate contact. However, no evidence of gradual unlocking of the interface or transient deformation has yet been found in the seismicity rate. To address this question, we develop a dense earthquake catalog covering 15 months preceding the mainshock and derived from the continuous waveform data set recorded by the Integrated Plate Boundary Observatory Chile (IPOC) and Iquique Local Network (ILN) networks. After declustering the seismicity, a space-time analysis highlights a large-scale acceleration of the seismicity along the interface accompanied by a deceleration of intermediate-depth earthquakes. We demonstrate the existence of a seismic quiescence downdip of the mainshock rupture before the July 2013 cluster. We propose that this seismic quiescence potentially highlights fluid circulation and/or aseismic motion along upper-plate crustal fault(s).

1. Introduction

Chile is well known for its intense seismic activity across the country where the largest earthquake ever was recorded in Valdivia in 1960 (M_w 9.5) and one of the major event in recent times, the M_w 8.8 Maule earthquake in 2010 (Delouis et al., 2010; Vigny et al., 2011). The northern portion of the Chilean subduction, from the city of Arica (−18.5° N) to the Mejillones Peninsula (−23° N), has been spared from major earthquakes since 1877 (Comte & Pardo, 1991; Nishenko, 1991) and has long been considered a seismic gap. On 1 April 2014, the Iquique earthquake of moment magnitude 8.2 broke a section of this seismic gap with a maximum slip of about 8 m (Duputel et al., 2015; Jara et al., 2018; Lay et al., 2014; Liu et al., 2015; Meng et al., 2015; Ruiz et al., 2014; Yagi et al., 2014). This earthquake was preceded by a series of seismic clusters described by Schurr et al. (2014): The very first anomalous and shallow was reported on 23 July 2013 offshore the city of Iquique and lasted for few days; the second cluster appeared in January 2014; the last cluster that happened on 16 March 2014 and started with a major upper-plate crustal foreshock of M_w 6.7 (Bedford et al., 2015) and lasted until the mainshock of 1 April. Ruiz et al. (2014) proposed that the last cluster of March 2014 was driven by a slow-slip event along the interface. Kato et al. (2016) detected several repeating earthquakes since July 2013, suggesting that each episodic cluster was driven by slow-slip, ultimately leading to the nucleation of the Iquique earthquake. Socquet et al. (2017) found evidence of these preparatory aseismic signals in the GPS data.

The unlocking of the interface by slow-slip events prior to major earthquakes has been observed at multiple subduction zones. Examples include the Tohoku-oki earthquake (Kato et al., 2012), the Arequipa earthquake (Ruegg et al., 2001), the Illapel earthquake (Huang & Meng, 2018; Poli et al., 2017), and more recently the Valparaiso sequence in April 2017 (Ruiz et al., 2017). Bouchon et al. (2016) observed a synchronization of high seismic moment release at both shallow (depth <40 km) and deeper (depth >80 km) portions of the subduction during the three seismic swarms preceding the Iquique earthquake and interpreted it as a deformation within the slab. Additionally, the slab-pull Tarapaca earthquake (M_w 7.1), which occurred in 2005

on an inherited normal fault landward of the Iquique earthquake (Peyrat et al., 2006), altered the large-scale plate motion and seismic behavior of the area, as demonstrated by Jara et al. (2017). In the later, the authors suggest a preparatory phase even longer than previously expected, comparable to the decadal timescale of the 2011 Tohoku-oki earthquake preparatory phase (Mavrommatis et al., 2014; Yokota & Koketsu, 2015), and more generally to subduction earthquakes through the initiation of stable slip (Bouchon et al., 2013).

Despite the important results concerning the preparatory phase of the Iquique earthquake, the potential of the IPOC (GFZ CNRS-INSU, 2006) and ILN (Cesca et al., 2009) networks has not yet been fully exploited in studying the seismicity during the months preceding the Iquique earthquake. The Centro Sismologico National (CSN) catalog contains 2–3 events per day (with a completeness magnitude of 4 Jara et al., 2017). A visual inspection of the data, however, shows numerous undetected events. By building a richer catalog, we will zero in on the microseismicity and aim to statistically highlight, in time and space, transients that could have played a key role in the preparatory phase of the Iquique earthquake.

In the next sections, we will present the method followed to build the seismic catalog (section 2). We will detail the declustering approach used to access the background seismicity (section 3) and introduce the statistical and original framework developed in this study to uncover the seismicity rate variations that can be associated with transient processes (section 4). Finally, section 5 is devoted to the discussion of the results.

2. Building the Catalog: Detection, Location, and Event Selection

The IPOC network was deployed in 2006 just before the M_w 7.7 Tocopilla earthquake (2007) in order to study the seismic gap of Northern Chile. The network was designed to capture a large range of deformation processes by using seismometers, strong-motion sensors, GPS, magnetotelluric sensors, creepmeters, and tiltmeters. This network represents a unique opportunity for studying the Northern Chilean subduction seismicity with 16 densely distributed stations that can record both interface and intraplate seismicity.

We built a new catalog from 13 December 2012 to 31 March 2014, following the method described in Ruiz et al. (2017). It combines different automated methods for detection and location of seismic events into three steps:

1. first detection on continuous data,
2. relocation of events detected, and
3. event selection.

For Step 1, we selected seven stations (Figure 1) that remained operational over the longest time period before the Iquique earthquake. We obtained a first set of detections with the BackTrackBB method (Poiata et al., 2016, 2018) applied to the vertical components with a 1-D *P*-wave velocity model. This method constructs kurtosis-based characteristic functions from the signal filtered at different frequency bands in order to highlight time-frequency features. Here, we used 10 narrow frequency bands between 5 and 50 Hz (using a logarithm spacing, the bands are centered around 5, 6.5, 8, 11, 14, 18, 23.2, 30, 38, and 50 Hz). The cross-correlation of each pair of characteristic functions is then backprojected onto a 3-D time-delay grid. In the original paper of Poiata et al. (2016), the detection of a seismic event is declared if the maximum of the stack of the time-delay grid —also called the source location function (SLF)—overcomes a threshold value of 0.7.

During this preliminary detection step, we choose to normalize the SLF to 1 and raise it to the power 18. This significantly reduces the scattering of the SLF for coherent seismic sources in the window of analysis and allows us to use the size of its 3-D error ellipsoid as a detection-trigger parameter (semiaxis smaller than 100 km) (see supporting information Figure S1). When there is no coherent seismic source observed in the data, the SLF remains scattered, which corresponds to a larger 3-D error ellipsoid (see Figure S2). This step greatly improves the number of detected events with low signal-to-noise ratio; however, it also implies many false detections that need to be removed later in the process. During Step 1, we obtained a total of 62,054 detections. In Step 2, we used all available stations and were able to differentiate *P* and *S* waves with a polarization analysis based on a singular value decomposition following Rosenberger (2010) (see Figure S3). In order to improve the location of the detected events, we relocate these events anew with BackTrackBB applied to the three components (see Figure S4).

To locate earthquakes, we use a 1-D velocity model proposed by Dorbath et al. (2008). To properly recover the geometry of the subduction at these latitudes, we incorporated the slab model of SLAB1.0

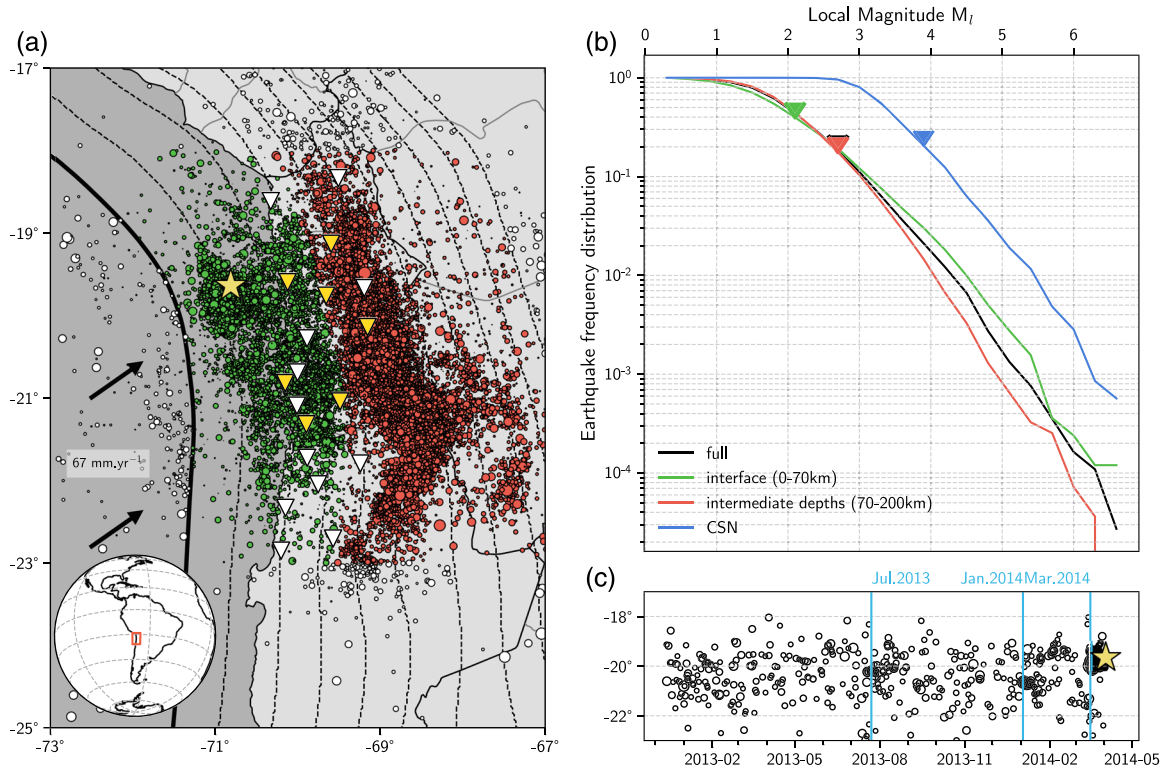

Figure 1. Earthquake catalog for Northern Chile from 12 December 2012 to 31 March 2014. (a) Location of the 35,371 earthquakes extracted from the IPOC/ILN data set. The black arrows point the direction of convergence at a rate of 67 mm yr^{-1} (Vigny et al., 2009). The solid black line marks the trench separating the Nazca and South American plates while the dashed lines are the isodepth profile each 20 km depth following the Slab 1.0 model (Hayes et al., 2012). The yellow star indicates the location of the Iquique earthquake. The triangles are the stations used in this work; their color indicates if it was used during the detection and location phases (yellow) or location phase only (white). The events are shown as circles and their size scales with their local magnitude. Green and red events constitute respectively the interface and the intermediate-depth catalogs, while white-colored events are discarded for this study. (b) Earthquake frequency distribution. Each line corresponds to a different earthquake catalog. The completeness magnitude of the presented catalog is 2.6 (CSN $M_c = 3.8$) with a b value of 0.89 (CSN $b = 0.85$). The triangles represent the completeness magnitudes of each catalog. (c) Latitude-time representation of the interface seismicity (M_L 3.0$^+$) prior to the mainshock. The vertical blue lines mark the three seismic clusters of July 2013 and January and March 2014.

(Hayes et al., 2012). We finally relocate every detection in Step 3 with the NonLinLoc program (Lomax et al., 2000; Lomax, 2005) in order to obtain a probability density of location, allowing us to select/discard events according to the size of their 68% error ellipsoid. The average length of the minor, intermediate, and major (mostly associated to the vertical axis) semiaxes is respectively 5 ± 5 km with 9.5% above 10 km, 10 ± 10 km with 26% above 10 km, and 23 ± 25 km with 59% above 10 km (see Figures S5 and S6). As the velocity model used here is poorly resolved at depth, we consider the 3-D-ellipsoid projected on the horizontal plane to select the event for the final catalog.

As we use now the 2-D 68% error ellipsoid, the new average length of the minor and major semiaxes is respectively 7 ± 11 km with 15% above 10 km and 22 ± 46 km with 40% above 10 km. We discarded events that have a 2-D ellipsoid with semiaxis length greater than 10 km. This threshold represents the best compromise between the number of events kept and the maximum length of the 2-D ellipsoid (see Figures S7 and S8).

We kept 35,371 earthquakes to build the final catalog between −22.5° N and −18.5° N and between −72° E and −66° E, in accordance with the latitude range of the network. As a comparison, 3,503 events are in the CSN catalog for the same period and the same area. We computed the local magnitude, M_L, for each event, based on the original work of Richter (1935):

$$M_L = \log(A_{WA}) - 5.35 + 0.42 \times \log(\Delta) + 5.10^{-3} \times \Delta. \quad (1)$$

A_{WA} is the maximum amplitude of displacement, in micron, after convolving the signal with the instrumental response of a Wood-Anderson seismometer. Δ is here the hypocentral distance. We lowered the completeness magnitude from 4.0 for the CSN to 2.6 (Figure 1b).

With the aim of studying the spatiotemporal variations of the seismicity, we distinguish two areas: the contact between the Nazca and South American plates that begins, for Northern Chile, at the trench to the downdip extent of the seismogenic zone at approximately 50–60 km depth (Béjar-Pizarro et al., 2010) and the interface below the seismogenic zone. To account for the weak resolution in depth of earthquake locations while still isolating each area, we extracted isodepth profiles from SLAB1.0 (Hayes et al., 2012) at 0, 70, and 200 km depth in order to build longitudinal boundaries and use them for dividing the catalog into subsets. The *interface* catalog contains 7,211 (1,447 with $M_L \geq 2.1$ for the interface) earthquakes between 0 and 70 km depth; the *intermediate depths* catalog contains 26,962 earthquakes (4,445 with $M_L \geq 2.6$ for intermediate depths) between 70 and 200 km isodepths (Figure 1).

It is important to note that two stations went missing: PB01 from 5 December 2013 to 1 January 2014 and PB02 from 25 December 2013 to 1 January 2014. Since the detection capacity of the BackTrackBB method depends on the network coherency (and thus directly on the network geometry), we do not analyze this time period.

3. Declustering of the Catalog: Nearest-Neighbor Distance

Seismicity is composed of mainshocks and their aftershocks. These mainshocks constitute the so-called background seismicity and are related to the stress field on the faults. Analysis of the background seismicity rate is a powerful tool to reveal transient deformations (Marsan et al., 2013; Reverso et al., 2015, 2016). Among numerous declustering techniques (Van Stiphout et al., 2012), we selected the nearest-neighbor distance metric (NND) proposed by Baiesi and Paczuski (2004) because it is self-adapted to observed seismicity and does not use tuning parameters other than characteristics of each event (i.e., the magnitude, the location, and occurrence time). It also represents a good compromise between computational efficiency and stability of the results. It consists of the estimation of the distance η between each event j and any event i that precedes it. Thus, the nearest-neighbor event will be the event i that minimizes this distance:

$$\eta_{i,j} = t_{i,j} \times (r_{i,j})^{df} \times 10^{-bm_i}, \tag{2}$$

where $t_{i,j} = t_j - t_i$ in days, $r_{i,j} = |r_i - r_j|$ in kilometers, m_i is the local magnitude of the event i, df is the fractal dimension that we set to 2 because we consider that the seismicity is located on the subduction interface, and b from the Gutenberg-Richter law (here $b = 0.89$, Figure 1). Zaliapin et al. (2008) went further and introduced a rescaled time difference $T_{i,j}$ and distance $R_{i,j}$ for discriminating clustered and nonclustered events in order to account for both time and space in the η distribution:

$$\begin{aligned} \eta_{i,j} &= T_{i,j} \times R_{i,j} \\ T_{i,j} &= t_{i,j} \times 10^{-\frac{1}{2}bm_i} \\ R_{i,j} &= (r_{i,j})^{df} \times 10^{-\frac{1}{2}bm_i}. \end{aligned} \tag{3}$$

The η distribution of equation (2) of the intermediate-depth catalog is unimodal (Figure 2) and can be described with a logarithmic scale by a Weibull function following (Zaliapin et al., 2008; Zaliapin & Ben-Zion, 2013). Taking $x = \log(\eta)$, the Weibull function is

$$f(x|x_0, \lambda, k) = \begin{cases} k\lambda\left(\frac{x-x_0}{\lambda}\right)^{(k-1)} \exp\left[-\left(\frac{x-x_0}{\lambda}\right)^k\right] & x \geq x_0 \\ 0 & x < x_0 \end{cases}, \tag{4}$$

where $k > 0$ is the shape parameter, $\lambda > 0$ is the scale parameter of the distribution, and x_0 is the location parameter. We are able to determine the three parameters x_0, λ, and k, through the minimization of the L_2 norm.

The η distribution of the interface catalog is bimodal (Figure 2), as expected (Zaliapin et al., 2008; Zaliapin & Ben-Zion, 2013). To separate the two populations, we modeled the distribution in this particular case with a sum of a log-Gaussian function, $g(x) = a_0 \exp((x - x_0)/\sigma)$, and a Weibull function (equation (4)). We fit the whole distribution by minimizing the L_2 norm. We finally determine the threshold between the two populations as the local minimum of the Gaussian and the Weibull distributions. By doing this, we accept to include a portion of background seismicity into the clustered catalog and a portion of the clustered seismicity into the background catalog.

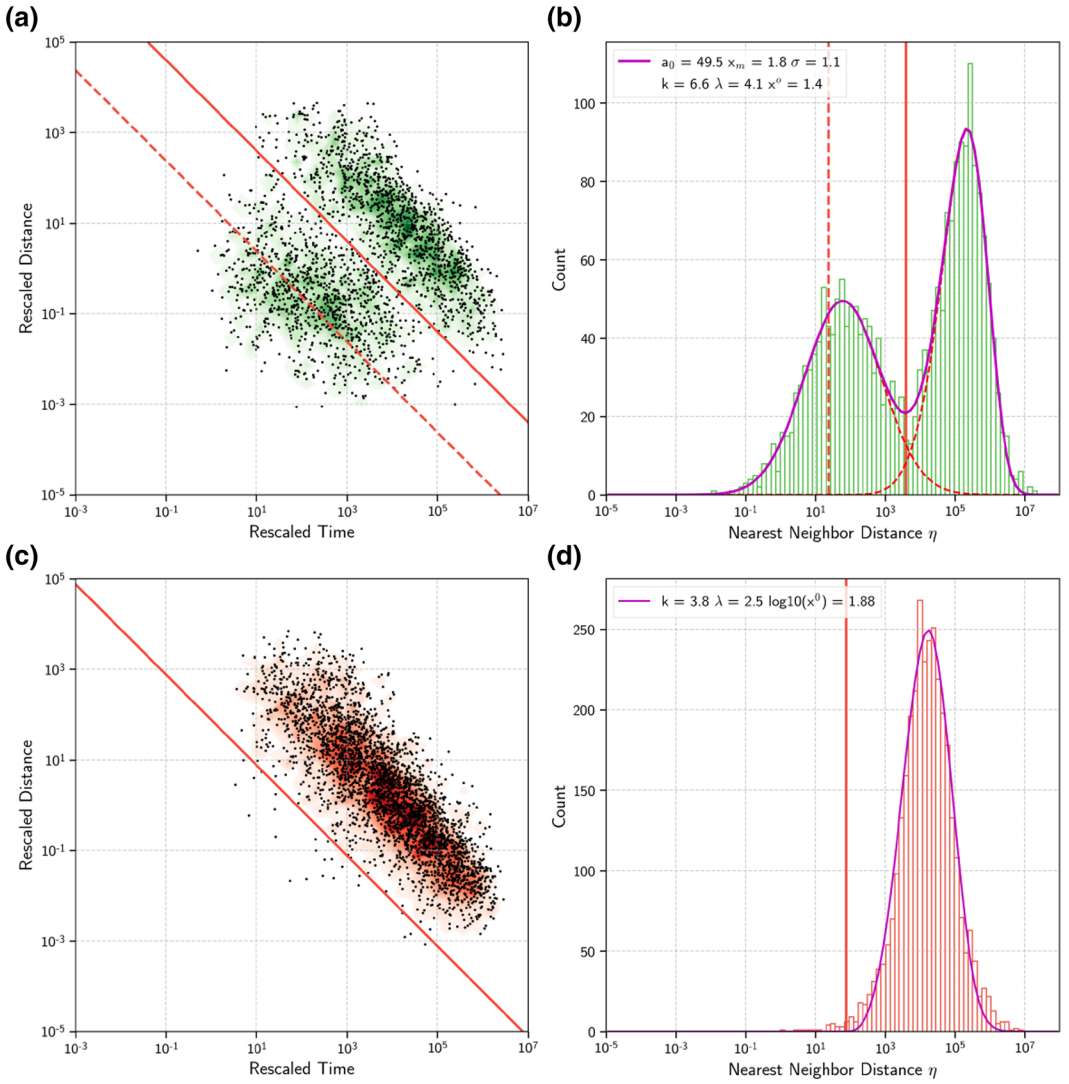

Figure 2. Nearest-neighbor distance applied to the seismicity of Northern Chile. (a) Joint distribution of the rescaled time T and distance R of the nearest-neighbor distance η. The intermediate-depth seismicity shows a single mode located along the line $\log(R) + \log(T) = 0.86$. (b) Histogram of the nearest-neighbor distance η, which may be modeled as a log-Weibull function (equation (4)). (c) and (d) show the same information but for the intermediate-depth catalog.

We clearly identify the three seismic clusters in the interface seismicity as aftershocks (Figure S9). In the following, we will study the background seismicity of the interface and intermediate-depth catalogs to detect spatiotemporal variations of their seismicity rate. We do not consider the background seismicity before 1 February 2013 due to edge effects: There are no sufficient number of background earthquakes to identify potential aftershocks (Marsan et al., 2017). This may lead to an overestimation of the background seismicity rate at the beginning of the catalog and ultimately induce a decrease of the seismicity rate as soon as the declustering algorithm is stabilized.

4. Analysis of the Background Seismicity

4.1. Reference Poisson Law

Siméon Denis Poisson introduced in 1838 the Poisson law to express the probability of a given number of events k occurring in a fixed interval of time T if these events occur with a known constant rate T_0 and independently of the time since the last event:

$$p(k, T, T_0) = \frac{1}{k!}\left(\frac{T}{T_0}\right)^k \exp\left(-\frac{T}{T_0}\right). \quad (5)$$

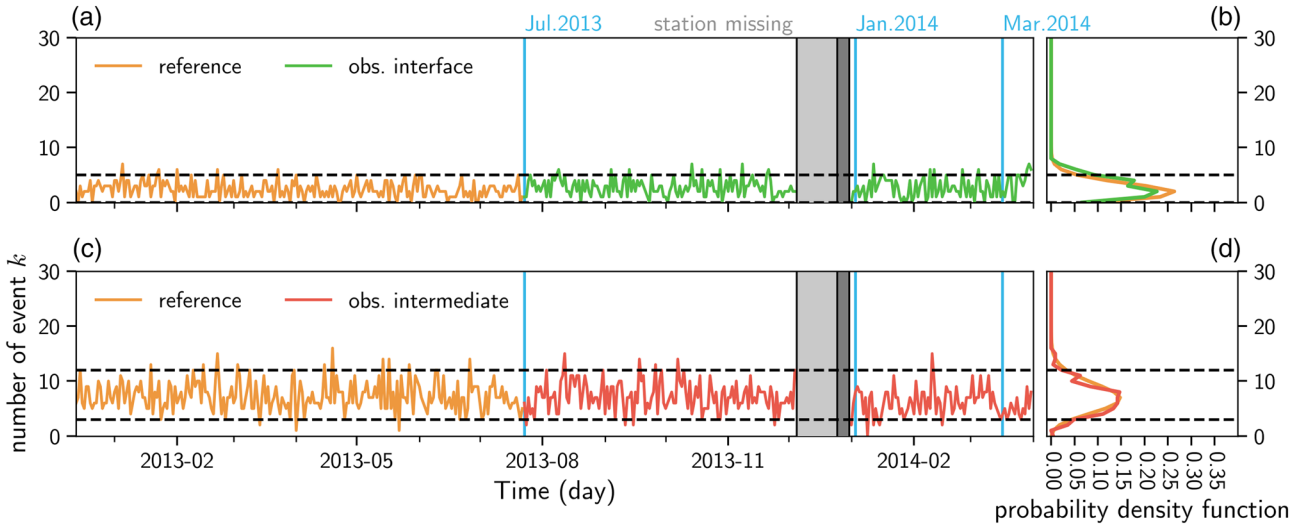

Figure 3. Earthquake counting distributions. (a) and (c) show the number of earthquakes per day, k. This number is plotted in orange for the reference period and in green (interface) or red (intermediate depths) for the observation period. The black dashed line corresponds to the 95% probability limit of the theoretical Poisson law deduced from the reference period. The vertical blue lines mark the three clusters that preceded the Iquique earthquake, and the gray rectangles display the period where two stations of the network went missing. The number of earthquakes occurring during these days is not taken into account in the following. (b) and (d) show respectively the probability density function for the observation period of the interface and the intermediate-depth seismicity, compared to the theoretical Poisson law.

Gardner and Knopoff (1974) demonstrated that a sequence of earthquakes in Southern California freed from aftershocks follows a Poisson law in time. Recently, Marsan et al. (2017) revealed aseismic transients along the Pacific Plate in Japan by comparing an initial background seismicity rate to an expected seismicity rate. The authors demonstrated that the declustering following a nearest-neighbor distance algorithm (Baiesi & Paczuski, 2004; Zaliapin et al., 2008) is consistent with the use of a space-time epidemic-type aftershock sequence (ETAS) model (Ogata, 1998); hence, it is suitable for studying the background seismicity variations through time. Here, we won't analyze the clustered seismicity.

4.2. Kolmogorov-Smirnov One-Sample Test

The Kolmogorov-Smirnov one-sample (KS1) test is a nonparametric statistical test commonly used to test whether an observed distribution is similar to a reference law (Gibbons & Chakraborti, 2011; Lehmann & Romano, 2006). Considering the distribution $o_n(k)$, with k the number of event per day, built from a set of observations measured during n days and the theoretical distribution $p(k)$. The test estimates the Kolmogorov-Smirnov criterion, denoted D_n, which is the maximum distance between the two cumulative distribution functions, noted $O_n(k)$ and $P(k)$, computed over n days:

$$D_n = \max_k |P(k) - O_n(k)|. \tag{6}$$

In seismology, the KS1 test has been used to assess the uniformity of declustered earthquake catalogs (Matthews & Reasenberg, 1988; Reasenberg & Matthews, 1988) but never to study seismicity rate variations. In the following, we won't consider the absolute value in equation (6), but we will keep the information held by the sign of the difference. This will offer an indication of an event deficit or an event excess. A negative D_n implies a greater probability for smaller number of event per day in regard to P, while a positive sign implies a greater probability for greater number of event per day. In the following, we refer to D_n as the event excess (a negative event excess is an event deficit). The null hypothesis, H_o: $O_n(k) = P(k)$, is considered rejected at significance level α if

$$|D_n| > \frac{K(\alpha)}{\sqrt{n}}, \tag{7}$$

where $K(\alpha)$ is a constant, which value can be found in tables (Gibbons & Chakraborti, 2011) or can be estimated from the Kolmogorov distribution (Kolmogorov, 1933). In the following, we will consider three levels of significance α: $K(\alpha = 0.68\%) = 0.96$, $K(\alpha = 0.95\%) = 1.36$, and $K(\alpha = 0.99\%) = 1.63$.

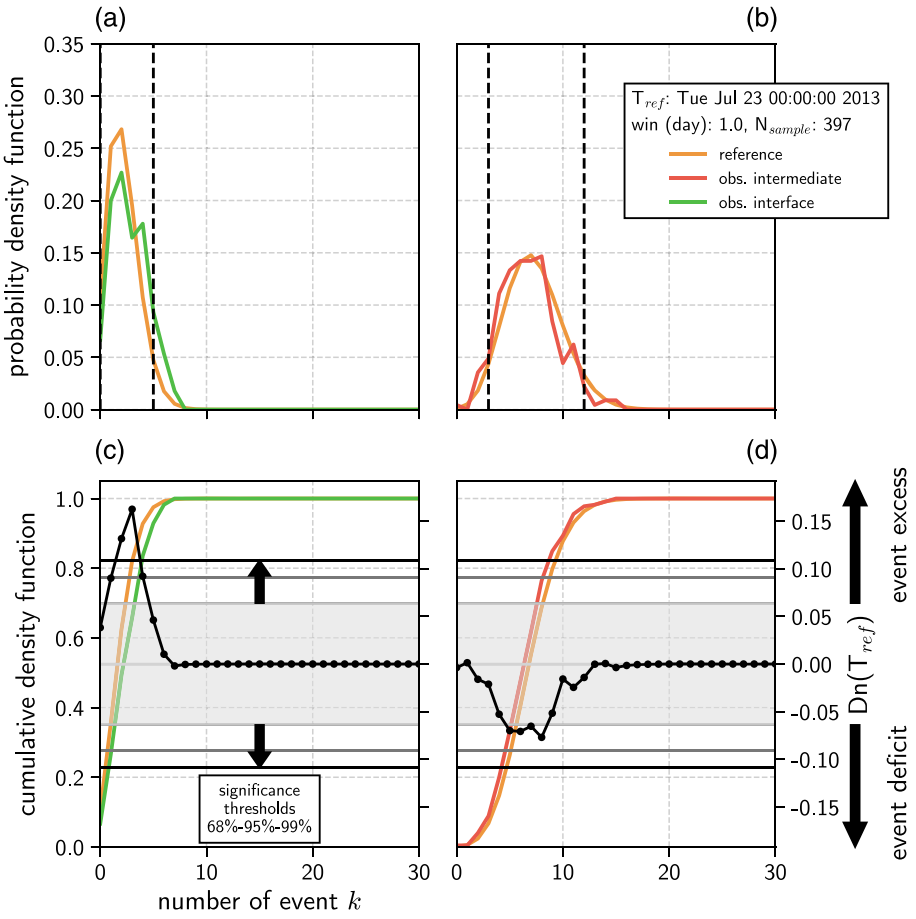

Figure 4. Kolmogorov-Smirnov one-sample test. (a) and (b) show the probability density functions of the reference (orange) and the observation periods (green and red) for the interface and intermediate-depth background seismicity. The black dashed lines correspond to the 95% probability limit of P_{ref}. (c) and (d) present the corresponding cumulative density functions. The dotted black line is the difference between P_{ref} and F_{obs}. The light gray, dark gray, and black contour lines represent the level of significance respectively at 68%, 95%, and 99.9%. The two black arrows in (c) show the direction of increasing significance. For this particular T_{ref}, from 1 February until 23 July, only the interface background shows a value of D_n at significant level higher than 99.9%, hence rejecting the null hypothesis that both distributions are equivalent.

One cannot assess which period corresponds to the *stable* seismicity rate especially for a catalog of this size (473 days). In the following analysis, we simply count the number of earthquakes per day. We consider that a sampling of $T = 1$ day is enough to have both a sufficient number of samples and a sufficient number of events per window. We now define a reference time period T_{ref} that determines the reference cumulative distribution ($P(k)$ in equation (6)) and then compare the time period $O_n(k)$ following T_{ref} to detect any statistically significant relative changes in the seismicity rate.

We begin by fixing T_{ref}: from 1 February until 23 July 2013, the day of the first cluster prior to the Iquique earthquake. We infer an average interevent time of $T_0 = T_{\text{ref}}/N_{\text{ref}}$, with N_{ref} the total number of events observed during T_{ref} for both the interface and intermediate-depth declustered catalogs. We compute the reference Poisson probability density function, p_{ref}, following equation (5). In a similar way, we count the number of earthquakes per day from the end of the reference period until 1 April 2014, the time of the Iquique earthquake. As mentioned above, we remove all days corresponding to the time periods when not all seven stations were operating ($n = 282$ remaining days) to obtain the two distributions of daily earthquake counts $o_{\text{obs}}(k)$ (Figure 3).

Next, we tested with a KS1 test, the null hypothesis H_0: $P_{\text{ref}}(k) = O_{\text{ref}}(k)$, put simply, is the theoretical Poisson law p_{ref} significantly similar to the observed distribution o_{ref}? Using a theoretical Poisson law p_{ref} allows us to overcome the problem of the reduced number of samples (days) of o_{ref}, the observed distribution during the

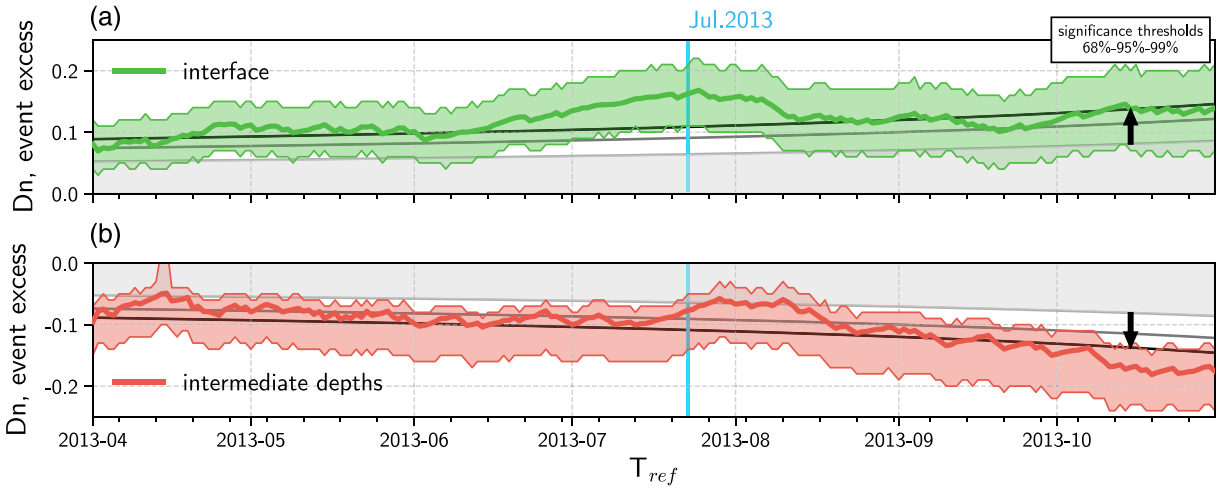

Figure 5. Kolmogorov-Smirnov one-sample test for different reference time periods T_{ref}. (a) and (b) show the evolution of the event excess or deficit D_n by changing T_{ref} respectively for the interface (green) and intermediate-depth (red) background catalogs. The lighter colors represent the 95% confidence intervals estimated by bootstrap resampling (2,000 populations). The light gray, dark gray, and black contour lines represent the level of significance respectively at 68%, 95%, and 99.9%, while the gray area represents the region of no significance. The two black arrows show the direction of increasing significance. The vertical blue line marks the first cluster of 23 July 2013.

reference period, and rather consider an infinite number of samples with p_{ref}. This test shows (Figure S10) that we cannot reject the null hypothesis H_0 and thus confirms that the cumulative distribution functions P_{ref} and O_{ref} are not distinguishable from one another. In the following, we measure the observed earthquake count distributions, $o_n(k)$, starting from 23 July 2013, the time of the first cluster, to 31 March 2014, the day before the mainshock (Figure 3).

Another KS1 test is performed to evaluate the null hypothesis H_1: $P_{\text{ref}} = O_{\text{obs}}$ for both interface and intermediate-depth catalogs (Figure 4). The null hypothesis H_1 is rejected for the interface background catalog with a significance of more than 99%, suggesting a great increase of the global seismicity after this date. For the intermediate-depth catalog, we obtain a negative event excess D_n but only significant at 68%, which we won't consider sufficient to be interpreted.

4.3. Varying the Reference Period T_{ref}

While the T_{ref} in the previous section, spanning between 1 February and 23 July 2013, is justified by the initiation of the first cluster in July 2013, it remains an arbitrary parameter. We computed the KS1 test for a range of T_{ref} varying from 1 April 2013 until 1 October 2013 with a step of a day. We thus obtain an event excess D_n for each catalog at each possible T_{ref}. The results are shown in Figure 5. We observe a general and progressive increase of the event excess as T_{ref} increases, marked by a strong and significant acceleration around the time of July 2013 cluster for the interface catalog; the event excess appears to decrease over time at intermediate depths toward a more significant deficit for later T_{ref}. We additionally conducted similar tests for $T = 0.5$, 2, and 5 days. These tests, illustrated in Figures S11–S13, indicate that the choice of T does not significantly affect the results presented above.

4.4. Mapping the KS1 Test

Until now, we have only considered the full declustered catalogs, without taking spatial information (i.e., event locations) into account. To have an overview of the spatiotemporal evolution of both interface and intermediate-depth background catalogs, we apply the KS1 test at each node of a 2-D grid discretized every 5 km and consider the events that occurred with a 30 km radius of the center of each grid cell.

Based on the previous results of the event excess estimation for different reference period, still starting from 1 February 2013, we will consider two end values for T_{ref}: T^1_{ref} will last until 20 May 2013, which is before the largest acceleration for the interface declustered catalog and T^2_{ref}, until 23 July 2013, which is the time of the first cluster.

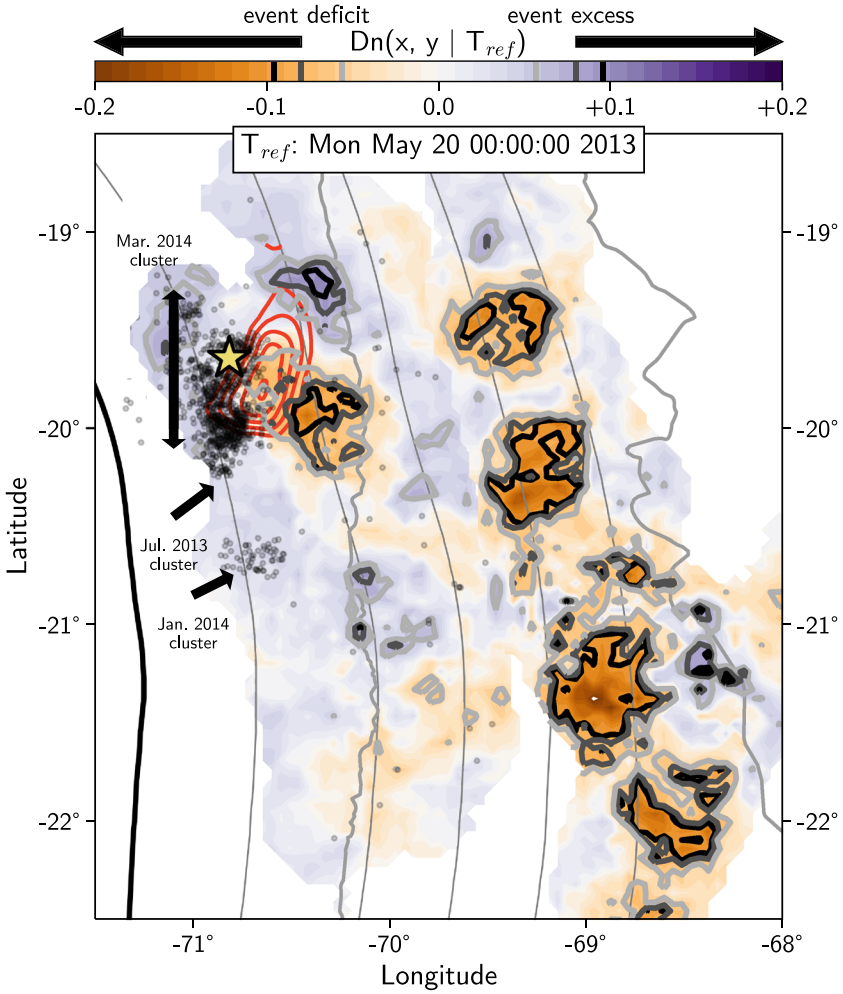

Figure 6. KS1 test estimated spatially the reference period: 1 February to 20 May 2013. The color scale represents the local event excess D_n. Negative values of D_n are associated to an event deficit after the time T_{ref}, while positive values are related to an event excess. The light gray, dark gray, and black contour lines represent the level of significance respectively at 68%, 95%, and 99.9%. The red contour lines represent the slip distribution of the Iquique earthquake (Ruiz et al., 2014). The black dots represent the clustered seismicity removed from the interface catalog. The black arrows point toward the location of the precursory clusters. The black dots represent the clustered seismicity removed from the interface catalog. The black arrows point toward the location of the precursory clusters. The thick black line is the trench, while thin gray lines are isodepths of the slab at 20, 40, 60, and 80 km deep.

4.4.1. T^1_{ref}: 20 May 2013

The spatial KS1 test for the interface background catalog shows striking patterns (Figure 6). We observe two offshore patches of event excess with significance over 68%, though only one is 95% significant (see bootstrap distribution for this region in Figure S14). We observe a broad region of event deficits with significance over 99% (see bootstrap distribution for this region in Figure S14). The spatial KS1 test highlights three large regions of event deficits of intermediate-depth seismicity with significance larger than 99% with one located at the latitudes of the Iquique mainshock and its major aftershock (Figure 6).

4.4.2. T^2_{ref}: 23 July 2013

The spatial KS1 test for the interface background catalog shows narrow patches of event excess with a significance over 95% (Figure 7). The quiescence previously observed is not significant anymore. Comparing this result with the result of T^1_{ref} implies that the event deficit occurs prior to 23 July. Concerning the intermediate-depth catalog (Figure 7), the spatial KS1 test still exhibits strong but narrower patches of event deficits at the latitudes of the Iquique mainshock (significance >95%).

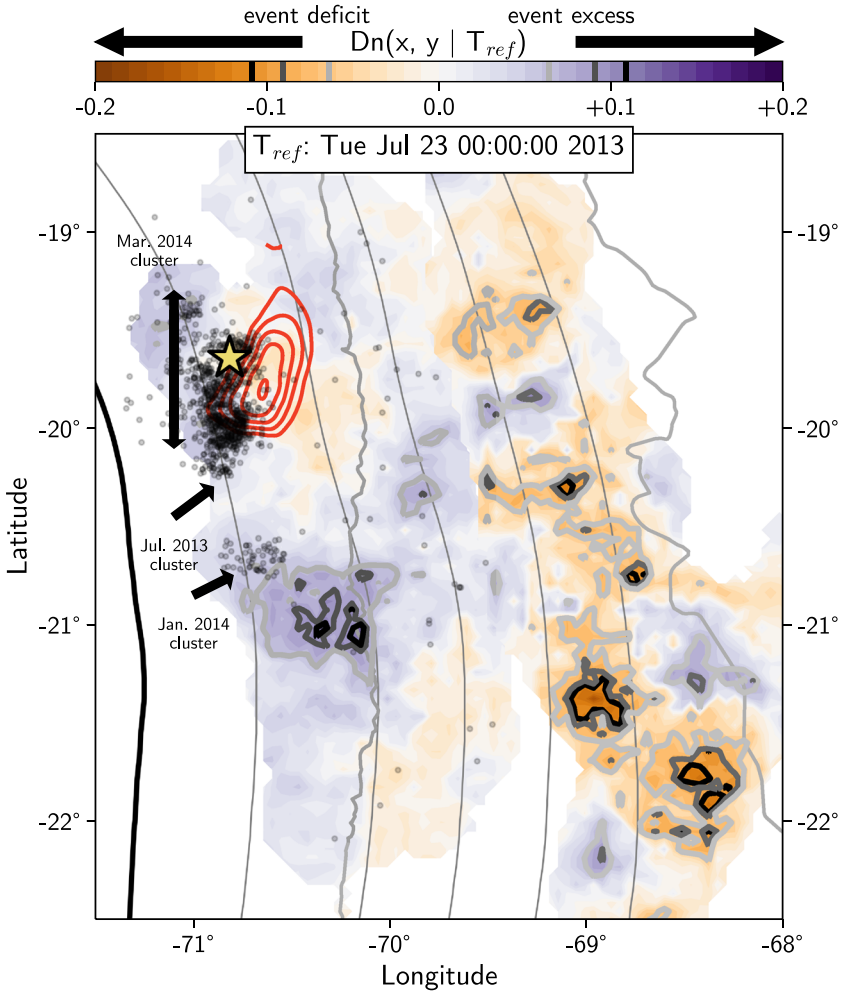

Figure 7. KS1 test estimated spatially for the reference period: 1 February to 23 July 2013. Same as Figure 6.

5. Discussion and Conclusions

We statistically investigated a potential large-scale destabilization of the plate interface in the north of Chile, as evidenced by significant relative changes in the background seismicity rates. We built a continuous seismic catalog from 12 December 2012 until 31 March 2014. The catalog's magnitude frequency distribution is described by a Gutenberg-Richter law with $b = 0.89$ and a completeness magnitude $M_c = 2.6$. We took particular care to select stations for the detection phase in order to avoid a bias in the estimation of the seismicity rate.

We investigated the declustered seismicity rate for two regions: the subducting plate interface ($z > 70$ km) and the intermediate depths further downdip (70km $> z >$ 200km). After the declustering of both catalogs with the nearest-neighbor distance algorithm (Baiesi & Paczuski, 2004; Zaliapin et al., 2008; Zaliapin & Ben-Zion, 2013), we searched for potential transient processes in these declustered catalogs following an original framework based on a KS1 test. First, we separated each catalog into two periods, the reference period and the observation period, before and after T_{ref}, which we varied from 1 February to 23 July 2013. We then compared both time periods in order to investigate any potential relative changes in the seismicity rate during the observation period. The KS1 test shows that the interface experienced a significant event excess of seismicity (>99% of significance) after the first cluster of July 2013, while the seismicity rate at intermediate depths seems to have remained constant. This first observation is in agreement with several studies that have proposed the unlocking of the plate interface during this time period (Kato et al., 2016; Schurr et al., 2014; Socquet et al., 2017).

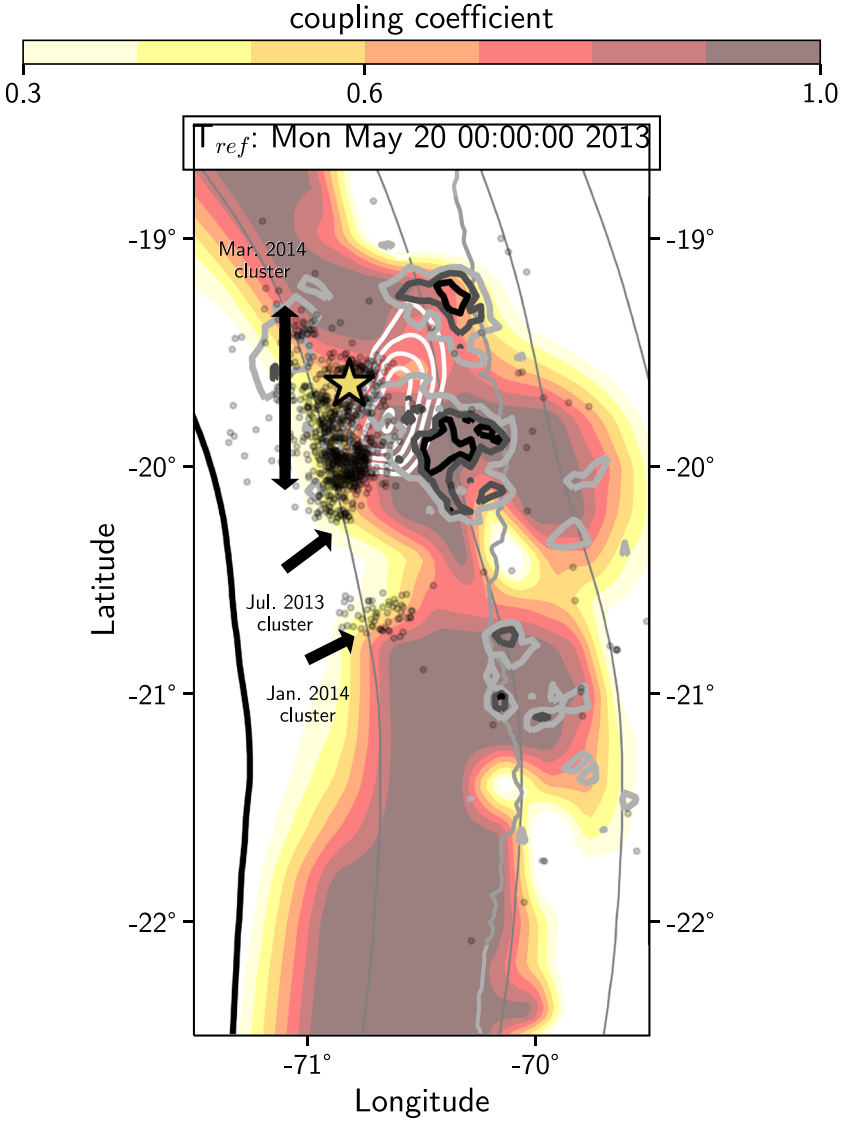

Figure 8. Seismic quiescience and local activation along the interface in relation to the coupling and the Iquique coseismic slip distribution. The color scale represents the interseismic coupling coefficient (Métois et al., 2016). The light gray, dark gray, and black contour lines represent the level of significance respectively at 68%, 95%, and 99.9% of the event excess and deficit observed in Figures 6 and 7). The dashed gray lines are isodepths of the slab at 20, 40, 60, and 80 km deep. The white contour lines represent the slip distribution of the Iquique earthquake (Ruiz et al., 2014).

We then applied the same test for all possible dates of T_{ref} between April 2013 and October 2013. This approach highlights a continuous increase of the event excess with the later dates of T_{ref} for the interface, while it is decreasing for the intermediate-depth seismicity. It is difficult to estimate a precise timing for these relative changes in the seismicity rate; however, an updip excess of events alongside a downdip deficit of events could be explained by the reduction of slab-pull tension due to the unlocking of the plate interface in the seismogenic zone, reducing the number of intermediate-depth earthquakes (Astiz & Kanamori, 1986; Dmowska & Lovison, 1988). However, this assumption needs to be confirmed by more detailed studies.

When we apply the KS1 test spatially to two different reference periods, striking patterns come out. It is interesting to note that, for a different T_{ref}, the spatial distribution of event excess D_n can be drastically different (Figures 6 and 7). For the interface and for T_{ref}: 1 February to 23 July 2013, we have a regional event excess D_n that overcomes the 99.9% of statistical significance (Figure 5); however, the map of spatial D_n for the same period of reference shows areas of negative D_n (which are not significant) (Figure 6). This is not surprising since we would have expected that the regional event excess D_n to represent a spatial average of

the region. We thus observe a large area of significant event deficit compensated by regions of significant and positive D_n.

The spatial distribution of event excess and its regional average are not contradictory, providing complementary insights on the background seismicity at two different scales: (1) the whole investigate and (2) at a 30 km scale. Concerning the difference observed between the two spatial KS1 tests, they do not constitute a paradox; it only demonstrates that this test is powerful to detect anomalies in the seismicity. By changing T_{ref}, we moved the anomalies from the observation to the reference period.

With this original framework based on the KS1 test and parameters relying only on observations, we are able to detect a global relative seismicity rate increase of the interface background seismicity while it relatively decreases at intermediate depths. We are also able to detect an event deficit or what we can call a "quiescence" downdip of the Iquique earthquake nucleation area (Figure 6) before the first cluster of July 2013, while the seismicity seems to have increased in different proportions in the surroundings of the mainshock.

Quiescence has been observed many times before large earthquakes (Katsumata, 2018; Ogata, 1992; Wiemer & Wyss, 1994; Wu & Chiao, 2006; Wyss & Habermann, 1988), but the potential mechanisms that are behind it are still poorly understood. It is interesting to observe that the quiescence appears in a region of high coupling coefficient (Figure 8) (Métois et al., 2016). This implies that a high-degree of coupling measured over decades (interseismic period) may vary at a smaller timescale, particulary when a megathrust earthquake is about to occur (Marsan et al., 2017). At the timescale of months, the space-time evolution of seismicity is probably the best indicator of short-term coupling variations on the subduction interface. For that, a precise relocation of the catalog presented in this work is needed. Future studies of migrations of seismicity, indirect evidence of dynamic changes in fluid pore pressure (Poli, 2017; Pasten-Araya et al., 2018; Yoon et al., 2009), or repeating earthquakes in the deeper region of the interface may give us clues to improve our understanding of the preparatory phase of the Iquique earthquake.

Through the lens of the microseismicity, our results confirm the large-scale unlocking of the Iquique interface, expanding from approximately −20.5° N to −19.5° N. We suggest that the Iquique mainshock may have been triggered by a stress build-up promoted by fluids flows and/or aseismic slip both updip and downdip and/or motion on upper-plate crustal fault(s). We highlight here the importance of building more complete and detailed catalogs, taking particular care of limiting artifacts, which may alter the seismicity rate. This work shows that statistical analysis of seismic catalogs is a powerful tool for providing indirect evidence of aseismic transients.

Acknowledgments
We want to thank P. Romanet who helped with the implementation of BackTrackBB and S. Ruiz and M. Bouchon for interesting and constructive discussions and comments. We also thank everyone who have contributed to the IPOC and ILN network. We would like to thank the editor Rachel Abercrombie and the reviewers Blandine Gardonio and Monika Sobiesiak for their comments and suggestions that greatly improved the manuscript. We thank F. Leyton and the CSN for the formula of the local magnitude. This work benefited from the supported of the SERA project, EU Horizon 2020, Grant Agreement No. 730900. The seismic catalog created for this study is available online (from https://doi.org/10.5281/zenodo.3597154).

References

Astiz, L., & Kanamori, H. (1986). Interplate coupling and temporal variation of mechanisms of intermediate-depth earthquakes in Chile, *76*(6), 1614–1622.

Béjar-Pizarro, M., Carrizo, D., Socquet, A., Armijo, R., Barrientos, S., Bondoux, F., et al. (2010). Asperities and barriers on the seismogenic zone in North Chile: state-of-the-art after the 2007 *M*w 7.7 Tocopilla earthquake inferred by GPS and InSAR data. *Geophysical Journal International*, *183*(1), 390–406.

Baiesi, M., & Paczuski, M. (2004). Scale-free networks of earthquakes and aftershocks. *Physical Review E*, *69*(6), 066106.

Bedford, J., Moreno, M., Schurr, B., Bartsch, M., & Oncken, O. (2015). Investigating the final seismic swarm before the Iquique-Pisagua 2014 M_W 8.1 by comparison of continuous GPS and seismic foreshock data. *Geophysical Research Letters*, *42*, 3820–3828. https://doi.org/10.1002/2015GL063953

Bouchon, M., Durand, V., Marsan, D., Karabulut, H., & Schmittbuhl, J. (2013). The long precursory phase of most large interplate earthquakes. *Nature Geoscience*.

Bouchon, M., Marsan, D., Durand, V., Campillo, M., Perfettini, H., Madariaga, R., & Gardonio, B. (2016). Potential slab deformation and plunge prior to the Tohoku, Iquique and Maule earthquakes. *Nature Geoscience*.

Cesca, S., Sobiesiak, M., Tassara, A., Olcay, M., Gnther, E., Mikulla, S., & Dahm, T. (2009). The Iquique local network and picarray.

Comte, D., & Pardo, M. (1991). Reappraisal of great historical earthquakes in the northern Chile and southern Peru seismic gaps. *Natural Hazards*, *4*(1), 23–44.

Delouis, B., Nocquet, J.-M., & Vallée, M. (2010). Slip distribution of the February 27, 2010 Mw = 8.8 Maule earthquake, central Chile, from static and high-rate GPS, InSAR, and broadband teleseismic data. *Geophysical Research Letters*, *37*, L17305. https://doi.org/10.1029/2010GL043899

Dmowska, R., & Lovison, L. C. (1988). Intermediate-term seismic precursors for some coupled subduction zones. *Pure and Applied Geophysics PAGEOPH*.

Dorbath, C., Gerbault, M., Carlier, G., & Guiraud, M. (2008). Double seismic zone of the Nazca plate in northern Chile: High-resolution velocity structure, petrological implications, and thermomechanical modeling. *Geochemistry, Geophysics, Geosystems*, *9*, Q07006. https://doi.org/10.1029/2008GC002020

Duputel, Z., Jiang, J., Jolivet, R., Simons, M., Rivera, L., Ampuero, J.-P., et al. (2015). The Iquique earthquake sequence of April 2014: Bayesian modeling accounting for prediction uncertainty. *Geophysical Research Letters*, *42*, 7949–7957. https://doi.org/10.1002/2015GL065402

GFZ CNRS-INSU (2006). GFZ German Research Centre for Geosciences; Institut des Sciences de l'Univers-Centre National de la Recherche CNRS-INSU (2006): IPOC seismic network.
Gardner, J. K., & Knopoff, L. (1974). Is the sequence of earthquakes in Southern California, with aftershocks removed, Poissonian. *Bulletin of the Seismological Society of America*, *64*(5), 1363–1367.
Gibbons, J. D., & Chakraborti, S. (2011). Nonparametric statistical inference. In *International encyclopedia of statistical science*, Springer, (pp. 977–979).
Hayes, G. P., Wald, D. J., & Johnson, R. L. (2012). Slab1. 0: A three-dimensional model of global subduction zone geometries. *Journal of Geophysical Research*, *117*, B01302. https://doi.org/10.1029/2011JB008524
Huang, H., & Meng, L. (2018). Slow unlocking processes preceding the 2015 Mw 8.4 Illapel, Chile, earthquake. *Geophysical Research Letters*, *45*, 3914–3922. https://doi.org/10.1029/2018GL077060
Jara, J., Sánchez-Reyes, H., Socquet, A., Cotton, F., Virieux, J., Maksymowicz, A., et al. (2018). Kinematic study of Iquique 2014 Mw 8.1 earthquake: Understanding the segmentation of the seismogenic zone. *Earth and Planetary Science Letters*, *503*, 131–143.
Jara, J., Socquet, A., Marsan, D., & Bouchon, M. (2017). Long-term interactions between intermediate depth and shallow seismicity in North Chile subduction zone. *Geophysical Research Letters*, *44*, 9283–9292. https://doi.org/10.1002/2017GL075029
Kato, A., Fukuda, J., Kumazawa, T., & Nakagawa, S. (2016). Accelerated nucleation of the 2014 Iquique, Chile Mw 8.2 earthquake. *Scientific Reports*, *6*, 24,792.
Kato, A., Obara, K., Igarashi, T., Tsuruoka, H., Nakagawa, S., & Hirata, N. (2012). Propagation of slow slip leading up to the 2011 Mw 9.0 Tohoku-oki earthquake. *Science*, 1215141.
Katsumata, K. (2018). Long-term seismic quiescences and great earthquakes in and around the Japan subduction zone between 1975 and 2012. In *Earthquakes and multi-hazards around the Pacific Rim* (vol. I, pp. 233–248): Springer.
Kolmogorov, A. (1933). Sulla determinazione empirica di una legge di distribuzione, Giornalo dell'Istituto Italiano degli Attuari 4, 461 (1933). Translated in A. N. Shiryayev. *Selected Works of A. N. Kolmogorov*, *2*.
Lay, T., Yue, H., Brodsky, E. E., & An, C. (2014). The 1 April 2014 Iquique, Chile, Mw 8.1 earthquake rupture sequence. *Geophysical Research Letters*, *41*, 3818–3825. https://doi.org/10.1002/2014GL060238
Lehmann, E. L., & Romano, J. P. (2006). *Testing statistical hypotheses*: Springer Science & Business Media.
Liu, C., Zheng, Y., Wang, R., & Xiong, X. (2015). Kinematic rupture process of the 2014 Chile Mw 8.1 earthquake constrained by strong-motion, GPS static offsets and teleseismic data. *Geophysical Journal International*, *202*(2), 1137–1145.
Lomax, A. (2005). A reanalysis of the hypocentral location and related observations for the Great 1906 California earthquake. *Bulletin of the Seismological Society of America*, *95*(3), 861–877.
Lomax, A., Virieux, J., Volant, P., & Berge-Thierry, C. (2000). *Probabilistic earthquake location in 3D and layered models*. In Advances in seismic event location (pp. 101–134): Springer.
Métois, M., Vigny, C., & Socquet, A. (2016). Interseismic coupling, megathrust earthquakes and seismic swarms along the Chilean subduction zone (38°–18° S). *Pure and Applied Geophysics*.
Marsan, D., Bouchon, M., Gardonio, B., Perfettini, H., Socquet, A., & Enescu, B. (2017). Change in seismicity along the Japan trench, 1990–2011, and its relationship with seismic coupling. *Journal of Geophysical Research: Solid Earth*, *122*, 4645–4659. https://doi.org/10.1002/2016JB013715
Marsan, D., Prono, E., & Helmstetter, A. (2013). Monitoring aseismic forcing in fault zones using earthquake time series. *Bulletin of the Seismological Society of America*.
Matthews, M. V., & Reasenberg, P. A. (1988). Statistical methods for investigating quiescence and other temporal seismicity patterns. *Pure and Applied Geophysics*, *126*(2-4), 357–372.
Mavrommatis, A. P., Segall, P., & Johnson, K. M. (2014). A decadal-scale deformation transient prior to the 2011 Mw 9.0 Tohoku-oki earthquake. *Geophysical Research Letters*, *41*, 4486–4494. https://doi.org/10.1002/2014GL060139
Meng, L., Huang, H., Bürgmann, R., Ampuero, J. P., & Strader, A. (2015). Dual megathrust slip behaviors of the 2014 Iquique earthquake sequence. *Earth and Planetary Science Letters*, *411*, 177–187.
Nishenko, S. P. (1991). Circum-Pacific seismic potential: 1989–1999. *Pure and Applied Geophysics*, *135*(2), 169–259.
Ogata, Y. (1992). Detection of precursory relative quiescence before great earthquakes through a statistical model. *Journal of Geophysical Research*, *97*(B13), 19,845–19,871.
Ogata, Y. (1998). Space-time point-process models for earthquake occurrences. *Annals of the Institute of Statistical Mathematics*, *50*(2), 379–402.
Pasten-Araya, F., Salazar, P., Ruiz, S., Rivera, E., Potin, B., Maksymowicz, A., et al. (2018). Fluids along the plate interface influencing the frictional regime of the Chilean subduction zone, northern Chile. *Geophysical Research Letters*, *45*, 10,378–10,388. https://doi.org/10.1029/2018GL079283
Peyrat, S., Campos, J., De Chabalier, J.-B., Perez, A., Bonvalot, S., Bouin, M.-P., et al. (2006). Tarapacá intermediate-depth earthquake (Mw 7.7, 2005, northern Chile): A slab-pull event with horizontal fault plane constrained from seismologic and geodetic observations. *Geophysical Research Letters*, *33*, L22308. https://doi.org/10.1029/2006GL027710
Poiata, N., Satriano, C., Vilotte, J. P., Bernard, P., & Obara, K. (2016). Multiband array detection and location of seismic sources recorded by dense seismic networks. *Geophysical Journal International*.
Poiata, N., Vilotte, J.-P., Bernard, P., Satriano, C., & Obara, K. (2018). Imaging different components of a tectonic tremor sequence in southwestern Japan using an automatic statistical detection and location method. *Geophysical Journal International*, *213*(3), 2193–2213. https://doi.org/10.1093/gji/ggy070
Poli, P. (2017). Creep and slip: Seismic precursors to the Nuugaatsiaq landslide (Greenland). *Geophysical Research Letters*, *44*, 8832–8836. https://doi.org/10.1002/2017GL075039
Poli, P., Jeria, A. M., & Ruiz, S. (2017). The Mw 8.3 Illapel earthquake (Chile): Preseismic and postseismic activity associated with hydrated slab structures. *Geology*, *45*(3), 247–250.
Reasenberg, P. A., & Matthews, M. V. (1988). Precursory seismic quiescence: A preliminary assessment of the hypothesis. *Pure and Applied Geophysics*, *126*(2-4), 373–406.
Reverso, T., Marsan, D., & Helmstetter, A. (2015). Detection and characterization of transient forcing episodes affecting earthquake activity in the Aleutian Arc system. *Earth and Planetary Science Letters*, *412*, 25–34.
Reverso, T., Marsan, D., Helmstetter, A., & Enescu, B. (2016). Background seismicity in Boso Peninsula, Japan: Long-term acceleration, and relationship with slow slip events. *Geophysical Research Letters*, *43*, 5671–5679. https://doi.org/10.1002/2016GL068524
Richter, C. F. (1935). An instrumental earthquake magnitude scale. *Bulletin of the Seismological Society of America*.
Rosenberger, A. (2010). Real-time ground-motion analysis: Distinguishing *P* and *S* arrivals in a noisy environment. *Bulletin of the Seismological Society of America*, *100*(3), 1252–1262.

Ruegg, J., Olcay, M., & Lazo, D. (2001). Co-, post- and pre(?)-seismic displacements associated with the Mw 8.4 Southern Peru earthquake of 23 June 2001 from continuous GPS measurements. *Seismological Research Letters*, *72*(6), 673–678.

Ruiz, S., Aden-Antoniow, F., Baez, J., Otarola, C., Potin, B., Campo, F., et al. (2017). Nucleation phase and dynamic inversion of the Mw 6.9 Valparaíso 2017 earthquake in Central Chile. *Geophysical Research Letters*, *44*, 10,290–10,297. https://doi.org/10.1002/2017GL075675

Ruiz, S., Metois, M., Fuenzalida, A., Ruiz, J., Leyton, F., Grandin, R., et al. (2014). Intense foreshocks and a slow slip event preceded the 2014 Iquique Mw 8.1 earthquake. *Science*.

Schurr, B., Asch, G., Hainzl, S., Bedford, J., Hoechner, A., Palo, M., et al. (2014). Gradual unlocking of plate boundary controlled initiation of the 2014 Iquique earthquake. *Nature*, *512*(7514), 299.

Socquet, A., Valdes, J. P., Jara, J., Cotton, F., Walpersdorf, A., Cotte, N., et al. (2017). An 8 month slow slip event triggers progressive nucleation of the 2014 Chile megathrust. *Geophysical Research Letters*, *44*, 4046–4053. https://doi.org/10.1002/2017GL073023

Van Stiphout, T., Zhuang, J., Marsan, D., Stiphout, V., Zhuang, J., & Marsan, D. (2012). Theme V-models and techniques for analyzing seismicity seismicity declustering. *CORSSA*.

Vigny, C., Rudloff, A., Ruegg, J.-C., Madariaga, R., Campos, J., & Alvarez, M. (2009). Upper plate deformation measured by GPS in the Coquimbo Gap, Chile. *Physics of the Earth and Planetary Interiors*, *175*(1-2), 86–95.

Vigny, C., Socquet, A., Peyrat, S., Ruegg, J.-C., Métois, M., Madariaga, R., et al. (2011). The 2010 Mw 8.8 Maule megathrust earthquake of central Chile, monitored by GPS. *Science*, *332*(6036), 1417–1421.

Wiemer, S., & Wyss, M. (1994). Seismic quiescence before the landers ($M = 7.5$) and big bear ($M = 6.5$) 1992 earthquakes. *Bulletin of the Seismological Society of America*, *84*(3), 900–916.

Wu, Y.-M., & Chiao, L.-Y. (2006). Seismic quiescence before the 1999 Chi-Chi, Taiwan, Mw 7.6 earthquake. *Bulletin of the Seismological Society of America*, *96*(1), 321–327.

Wyss, M., & Habermann, R. E. (1988). Precursory seismic quiescence. *Pure and Applied Geophysics*, *126*(2-4), 319–332.

Yagi, Y., Okuwaki, R., Enescu, B., Hirano, S., Yamagami, Y., Endo, S., & Komoro, T. (2014). Rupture process of the 2014 Iquique Chile earthquake in relation with the foreshock activity. *Geophysical Research Letters*, *41*, 4201–4206. https://doi.org/10.1002/2014GL060274

Yokota, Y., & Koketsu, K. (2015). A very long-term transient event preceding the 2011 Tohoku earthquake. *Nature Communications*, *6*, 5934.

Yoon, M., Buske, S., Shapiro, S., & Wigger, P. (2009). Reflection image spectroscopy across the Andean subduction zone. *Tectonophysics*, *472*(1-4), 51–61.

Zaliapin, I., & Ben-Zion, Y. (2013). Earthquake clusters in Southern California I: Identification and stability. *Journal of Geophysical Research: Solid Earth*, *118*, 2847–2864. https://doi.org/10.1002/jgrb.50179

Zaliapin, I., Gabrielov, A., Keilis-Borok, V., & Wong, H. (2008). Clustering analysis of seismicity and aftershock identification. *Physical Review Letters*, *101*(1), 018501.